

VILNIUS UNIVERSITY  
CENTER FOR PHYSICAL SCIENCES AND TECHNOLOGY

**Kęstutis Juškevičius**

**INVESTIGATION OF OPTICAL AND PHYSICAL PROPERTIES  
OF DIELECTRIC THIN FILMS AND OPTIMISATION OF THEIR  
DEPOSITION TECHNOLOGIES**

Summary of doctoral thesis,  
Physical Sciences, Physics (02P)

Vilnius, 2014

Dissertation was prepared in 2009-2013 at the Center for Physical Sciences and Technology (CPST).

**Scientific supervisor:**

Dr. Ramutis Drazdys (Center for Physical Sciences and Technology (Lithuania), Physical Sciences - 02P).

**Doctoral thesis will be defended at the Center for Physical Sciences and Technology in the senate of Physical Sciences:**

**Chairman:**

Prof. habil. dr. Valerijus Smilgevičius (Vilnius University, Physical Sciences, Physics - 02P).

**Members:**

Prof. habil. dr. Artūras Jukna (Vilnius Gediminas Technical University, Physical Sciences, Physics - 02P);

Dr. Rimantas Grigonis (Vilnius University, Physical Sciences, Physics - 02P);

Dr. Darius Milčius (Lithuanian Energy Institute, Technology Sciences, Material Engineering - 08T);

Dr. Kęstutis Regelskis (Center for Physical Sciences and Technology, Physical Sciences, Physics - 02P).

**Official opponents:**

Dr. Bonifacas Vengalis (Center for Physical Sciences and Technology, Physical Sciences, Physics - 02P);

Prof. habil. dr. Julius Dudonis (Kaunas Technological University, Physical Sciences, Physics - 02P).

This thesis will be under open consideration on 4th of September, 2014 10 a.m. at the hall of CPST Institute of Physics.

Address: Savanorių ave. 231, LT-02300 Vilnius, Lithuania.

Summary of doctoral thesis was distributed on 28<sup>th</sup> of July, 2014.

Doctoral thesis is available at libraries of CPST and Vilnius University.

VILNIAUS UNIVERSITETAS  
VALSTYBINIS MOKSLINIŲ TYRIMŲ INSTITUTAS  
FIZINIŲ IR TECHNOLOGIJOS MOKSLŲ CENTRAS

KĘSTUTIS JUŠKEVIČIUS

**PLONŲJŲ DIELEKTRINIŲ SLUOKSNIŲ OPTINIŲ IR  
FIZINIŲ SAVYBIŲ TYRIMAS BEI JŲ FORMAVIMO  
TECHNOLOGIJŲ OPTIMIZAVIMAS**

Daktaro disertacija  
Fiziniai mokslai, fizika (02 P)

Vilnius, 2014

Disertacija rengta 2009-2013 metais Fizinių ir technologijos mokslų centro lazerinių technologijų skyriuje.

**Mokslinis vadovas:**

Dr. Ramutis Drazdys (Fizinių ir technologijos mokslų centras, fiziniai mokslai, fizika -02P).

**Disertacija ginama Vilniaus universiteto Fizikos mokslų krypties taryboje:**

**Pirmininkas:**

Prof. habil. dr. Valerijus Smilgevičius (Vilniaus universitetas, fiziniai mokslai, fizika - 02P).

**Nariai:**

Prof. habil. dr. Artūras Jukna (Vilniaus Gedimino technikos universitetas, fiziniai mokslai, fizika – 02P);

Dr. Rimantas Grigonis (Vilniaus universitetas, fiziniai mokslai, fizika – 02P);

Dr. Darius Milčius (Lietuvos energetikos institutas, technologijos mokslai, medžiagų inžinerija – 08T);

Dr. Kęstutis Regelskis (Fizinių ir technologijos mokslų centras, fiziniai mokslai, fizika – 02P).

**Oponentai:**

Dr. Bonifacas Vengalis (Fizinių ir technologijos mokslų centras, fiziniai mokslai, fizika – 02P);

Prof. habil. dr. Julius Dudonis (Kauno technologijos universitetas, fiziniai mokslai, fizika – 02P).

Disertacija bus ginama viešame Fizikos mokslo krypties tarybos posėdyje 2014 m. rugsėjo mėn. 4 d. 10 val. FTMC Fizikos instituto salėje.

Adresas: Savanorių pr. 231, LT-02300 Vilnius, Lietuva.

Disertacijos santrauka išsiuntinėta 2014 m. liepos 28 d.

Disertaciją galima peržiūrėti Vilniaus universiteto ir FTMC bibliotekose.

# Contents

Introduction.....	6
Relevance.....	7
The scientific tasks of this work .....	9
Novelty and importance.....	10
Statements to be defended .....	10
List of the author’s publications related to thesis .....	12
Summary of doctoral thesis .....	13
Chapter 1. Literature survey .....	13
Chapter 2. Experimental techniques .....	13
Chapter 3. Investigation of Beilby (polished) layer .....	17
Chapter 4. Influence of etching time on surface roughness and LIDT .....	18
Chapter 5. Coating designs with variable gradient refractive index .....	19
Chapter 6. Investigations of $ZrO_2$ thin films deposited by reactive magnetrons sputtering ..	23
Chapter 7. Investigation of $Nb_2O_5/SiO_2$ mixture thin films deposited by reactive magnetron sputtering technique.....	27
Conclusions.....	30
References.....	32
Santrauka .....	36

## Introduction

In the doctoral thesis experimental results are presented in 3 parts. In the first part we report an experimental investigation of subsurface damage (SSD) in conventionally polished fused silica (FS) substrates [1-3], which are widely used in laser applications and directly influence performances of optical elements. Subsurface damages are defined as residual digs and scratches, some of which are filled with polishing slurry and covered with so-called Bielby layer (polished layer). Acid etching procedure of FS substrates was developed, which allows removing polished layer and eliminating SSD [4-6]. Surface roughness and laser induced damage threshold (LIDT) measurements were performed to find correlation between the main surface properties as circumstantial evidence of elimination of SSD. Different durations of acid etching have been used to study LIDT of FS substrates. These experiments revealed that the optimal etching time is ~1 min for a given acid concentration. Laser induced damage threshold of etched FS samples increased ~4 times.

In second part, we investigate a LIDT in  $\text{LiB}_3\text{O}_5$  (LBO) crystals coated with different types of (single AR@355 nm and triple AR@355+532+1064 nm wavelength) anti-reflective coatings while optimizing the refractive index. All these coatings were produced of different oxide materials ( $\text{ZrO}_2$ ,  $\text{Al}_2\text{O}_3$ , and  $\text{SiO}_2$ ) and  $\text{ZrO}_2$ - $\text{SiO}_2$  mixtures by using the ion beam sputtering (IBS) deposition technique. The Noch filter with gradient refractive index profile were designed and deposited on FS substrate.

In third part, we present explorations of reactive magnetron sputtering technology for deposition of  $\text{ZrO}_2$  and  $\text{Nb}_2\text{O}_5/\text{SiO}_2$  mixture thin films at low substrate temperature. A high deposition rate (64 % of the pure Zr metal rate) process of zirconium oxide is obtained by employing active feedback reactive gas control which creates a stable and repeatable deposition processes in the transition region. Substrate heating at 200°C was found to have no significant effect on the optical  $\text{ZrO}_2$  film properties. The addition of nitrogen to a closed-loop controlled process was found to have mostly negative effects in terms of deposition rate and optical properties. Constant reactive gas flow  $\text{O}_2$  gas regulated  $\text{ZrO}_2$  film deposition is slow and requires elevated (200°C) substrate temperature or post-deposition annealing to reduce absorption losses. X-ray diffraction analysis showed crystalline  $\text{ZrO}_2$

films consisted of monoclinic + tetragonal phases when produced in Ar/O<sub>2</sub> atmosphere and monoclinic + rhombohedral or a single rhombohedral phase when produced in Ar/O<sub>2</sub> + N<sub>2</sub>.

Niobia/silica mixture thin films were deposited using a reactive DC - RF magnetron co-sputtering of Nb and Si metal targets at room temperature. The reactive gas flow during the sputtering processes was controlled by constant reactive gas flow or by an active feedback process control system. The deposition rates of an Nb<sub>2</sub>O<sub>5</sub> and SiO<sub>2</sub> layers higher by 61% and 137%, respectively, were obtained using the latter technique. All mixture films produced in this study had amorphous structure. Substantially less inhomogeneity of mixture coatings was found in feedback controlled reactive sputtering processes.

## Relevance

It is well known that the conventional CeO<sub>2</sub> abrasive polishing technique, which relies on a normal load applied to an abrasive particle, cause material removal and generates scratches and subsurface damage (SSD) of fused silica glass [1-3]. Subsurface damages are defined as residual digs and scratches, some of which are filled with polishing slurry and covered with so-called Bielby layer (polished layer) [7-9]. These hidden and un-hidden scratches created during grinding and polishing behave like a combination of two phenomena: light absorption in scratches filled polishing slurry, especially in UV wavelength of laser radiation [10-12] and enhancement of electric field of laser pulses in surface micro-cracks [13, 14]. The strong effect of reduction in scratches and SSD was reached by using magnetorheological finishing process [4, 15, 16]. However, this very complex finishing procedure did not eliminate the problem of SSD. For this reason, various post-polishing techniques were suggested by many authors during the past decade: 1) wet etching in hydrofluoric acid/ammonium fluoride-based solutions (HF/NH<sub>4</sub>F) [4-6, 17], 2) leaching in concentrated nitric acid and hydrogen peroxide (HNO<sub>3</sub>/H<sub>2</sub>O<sub>2</sub>) solution [18], 3) ion etching [19, 20] and 4) UV laser conditioning [16, 21].

Designs comprising a stack of periodically alternating high and low (HL) refractive index dielectric layers of  $\lambda/4$  optical thicknesses are commonly used in optical components [22, 23]. Composite thin films consisting of mixtures of two or more materials exhibit

unique optical properties not observed in conventional materials. This has motivated the development of complex mixed structures, such as gradient refractive index coatings [24, 25] for laser applications. For example, the rapid development of femtosecond laser technology has led to a requirement for coatings of significantly higher complexity and multifunctionality. Also, structures highly resistant to laser radiation and of more sophisticated design, in which the refractive index varies smoothly and periodically through the film thickness became on demand [26-28]. The employment of the mixed and graded coating composites avoids the presence of discrete layer interfaces and offer some improvements in optical properties compared to classical HL designs, such as reduction of optical losses [29] and residual stress [30-32]. Besides loss reduction, stress control and refractive index tunability, such coatings offers a viable alternative to traditional coating materials when the improvement of Laser Induced Damage Threshold (LIDT) is required. In femtosecond laser pulse regimes, the LIDT shows strong band gap dependence [24]. A recent paper demonstrated that nanosecond and subpicosecond LIDT of mixed oxide films depends not only on precursors (defects), but also on the width of the optical band gap that the coating material exhibits [33].

The laser-induced damage of coated nonlinear crystals (in example, LBO or other optical material) is frequently a limiting factor in the high-power laser applications. LBO crystal is an excellent nonlinear material highly transparent in a wide spectral range (from 160 to 3500 nm) that is typically used for frequency conversion [34]. On the other hand, LBO is also one of the most resistant materials to laser radiation [35]. However, it is necessary to deposit antireflection (AR) coatings on the crystal surfaces in order to reduce reflectance losses of fundamental and higher order generated harmonics [36]. It is also known, that LIDTs of coated LBO crystal surfaces are strongly dependent on the quality of surface polishing, which also affects the adhesion between coating and crystal and, furthermore, on the technology and materials of AR coatings [37]. Here, our research is mostly focused on design optimization and material selection for antireflective coatings.



Reactive Magnetron Sputtering (MS) deposition is a physical vapor deposition technology used widely in both production and in scientific investigations. Reactive MS processes without appropriate process control can be accompanied by problems, such as uncontrolled transition to a fully poisoned target state (with a significant drop in deposition rate) [38, 39], process drifts, arcing, poor run-to-run repeatability [40-42] and, as a result, deterioration of film and product properties. Arcing in reactive sputtering processes can be minimized by using medium frequency AC (40 - 100 kHz), radio frequency RF (13.56 MHz) or pulsed-Direct Current (p-DC) (20 - 350 kHz) power [43, 44].

The transition between ‘metal’ and ‘compound’ target states phenomena typically observed in reactive MS processes present an opportunity to improve compound film properties and deposition rate when employing appropriate process control hardware [39, 45, 46]. Despite advances in process control technology [39], the direct mass flow control (MFC) mode (i.e. constant reactive gas flow) is still often used for optical film deposition [47-49]; that typically means operation in a fully poisoned target state. Target voltage ( $V_T$ ) feedback-based closed-loop gas flow control is one of the most cost-effective methods to regulate reactive oxide thin film sputtering processes. However, it can be difficult to perform due to target voltage non-linearity, changes in signal direction and drifts in the case of Zr sputtering in an Ar/O<sub>2</sub> ambient.

## **The scientific tasks of this work**

The main aim of this work was to identify physical causes that limit optical component’s spectral properties and resistance to laser radiation as well as to optimize the final substrate preparation procedure and coating deposition technology.

To achieve this aim, the following tasks were established:

- To investigate the influence of surface roughness, subsurface damages and chemical composition on the resistance of the FS substrates to laser radiation.
- To develop an etching procedure of polished FS substrates that would remove subsurface damages and increase the resistance of optical components to laser radiation.

- To fabricate multilayer optical coatings so that the refractive index varied smoothly and periodically throughout the thickness of the film.
- To develop a simple process for reactive magnetron sputtering-based coating with  $ZrO_2$ .
- To develop, characterize and optimize a technique for high rate  $Nb_2O_5/SiO_2$  mixture deposition by using reactive magnetron sputtering.

## Novelty and importance

Acid etching procedure of FS substrates was developed, which allows removing polished layer and eliminating SSD. Laser induced damage threshold of bare etched FS samples was increased ~4 times and from 1.5 to 3 times of various optical components deposited by multilayer coatings. The application of this method was submitted to the State Patent Bureau of the Republic of Lithuania for a National patent.

We first showed that the use of ratio  $V_T/O^*$  (i.e. target voltage signal divided to oxygen plasma optical emission intensity) as a feedback signal, facilitates problem-free closed-loop process control and thereby permits operation in the forbidden part of the so-called ‘transition’ region.

The most of the experiments made in this work have a practical value, for example the magnetron sputtering technique, which allows fast and effective fabrication of the dielectric thin films suitable for the deposition of optical coatings.

## Statements to be defended

1. One minute acid etching in the 20% HF and 80%  $HNO_3$  solution allows to increase the laser induced damage threshold of etched fused silica substrates by a factor of 4. Chemical etching of optical substrates increases the resistance of antireflective, polarizing and beam splitting optical elements to the UV laser ( $\lambda=355nm$ ) radiation from 1.5 to 3 times.
2. Thin films composed of  $ZrO_2$  and  $SiO_2$  mixtures has less absorption loss in UV range than the layers composed of  $ZrO_2$  alone. This allows formation of optical coatings

more resistant to laser radiation and coatings with unique spectral properties: narrow area of high reflection and high transmission in the wide wavelength range.

3. The response of Zr target voltage is abnormal at the changing reactive gas flow during reactive magnetron sputtering process. The best optical properties of  $ZrO_2$  thin films were reached at the maximal value of target voltage in constant power sputtering regime.
4. Zr magnetron sputtering in the  $Ar+O_2$  atmosphere makes zirconium oxide to form polycrystalline monoclinic-tetragonal mixture phases. Sputtering in the  $Ar+O_2+N_2$  atmosphere, causes the formation of monoclinic-rhombohedral mixture phases or pure rhombohedral polycrystalline phase.
5.  $Nb_2O_5/SiO_2$  mixed oxide films, deposited by reactive magnetron sputtering, using two reactive gas control methods, are amorphous in structure. Their surface roughness depend only on the substrate roughness and do not depend on control method.  $Nb_2O_5/SiO_2$  mixture thin films, deposited using active-feedback controlled reactive sputtering process, have significantly reduced refractive index inhomogeneity compared to thin films deposited using constant reactive gas flow.

## List of the author's publications related to thesis

- I. K. Starke, L. O. Jensen, M. Jupé, D. Ristau, G. Abromavičius, **K. Juškevičius**, R. Buzelis, and R. Drazdys, "Investigation in oxide mixture coatings with adapted gradient index profiles," Proc. SPIE **7504**, 75040B (2009).
- II. G. Abromavičius, R. Buzelis, R. Drazdys, **K. Juškevičius**, S. Kičas, T. Tolenis, J. Mirauskas, M. Ščiuka, V. Sirutkaitis, and A. Melninkaitis, "Optical resistance and spectral properties of antireflective coatings deposited on LBO crystals by ion beam sputtering" Lith. J. Phys. **51**, 303-308 (2011).
- III. S. Liukaitytė, G. Batavičiūtė, E. Pupka, M. Ščiuka, I. Kraujalienė, D. Tumosa, A. Skrebutėnas, **K. Juškevičius**, T. Tolenis, S. Kičas, R. Drazdys, R. Buzelis, and A. Melninkaitis, "Effect of conventional fused silica preparation and deposition techniques on surface roughness, scattering, and laser damage resistance," Proc. SPIE 8530, (2012).
- IV. **K. Juškevičius**, R. Buzelis, S. Kičas, T. Tolenis, R. Drazdys, G. Batavičiūtė, E. Pupka, L. Smalakys, and A. Melninkaitis, "Investigation of subsurface damage impact on resistance of laser radiation of fused silica substrates," Proc. SPIE 8885, (2013).
- V. S. Kičas, G. Batavičiūtė, **K. Juškevičius**, T. Tolenis, R. Drazdys, R. Buzelis, and A. Melninkaitis, "Characterization and application of  $HfO_2$  -  $SiO_2$  mixtures produced by ion-beam sputtering technology," Proc. SPIE **8885**, (2013)
- VI. **K. Juškevičius**, M. Audronis, A. Subačius, R. Drazdys, R. Juškėnas, A. Matthews, and A. Leyland, "High-rate reactive magnetron sputtering of zirconia films for laser optics applications," Appl. Phys. A, 1-12 (2014)
- VII. M. Audronis, A. Matthews, **K. Juškevičius**, R. Drazdys, "Unlocking the Potential of Voltage Control for High Rate Zirconium and Hafnium Oxide Deposition by Reactive Magnetron Sputtering," Vacuum, 107, 159-163 (2014).
- VIII. **K. Juškevičius**, M. Audronis, A. Subačius, S. Kičas, T. Tolenis, R. Buzelis, R. Drazdys, M. Gaspariūnas, V. Kovalevskij, A. Matthews and A. Leyland, „Fabrication of  $Nb_2O_5$ - $SiO_2$  mixtures by reactive DC - RF magnetron co-sputtering technique“, Thin Solid Films (2014) (submitted)

### Others publications:

- I. S. Survilienė, A. Češūnienė, R. Juškėnas, A. Selskienė, D. Bučinskienė, P. Kalinauskas, **K. Juškevičius**, and I. Jurevičiūtė, "The use of trivalent chromium bath to obtain a solar selective black chromium coating," Appl. Surf. Sci. 305, 492-497 (2014).

# Summary of doctoral thesis

Doctoral thesis contains 7 chapters.

## Chapter 1. Literature survey

In this chapter, the basics of the light dispersion, interference and absorption in dielectric material are reviewed. The interference phenomena in thin films and various constructions of multilayer optical coatings are discussed. The main fabrication methods of dielectric thin films such as electron beam evaporation (EBE), ion beam sputtering (IBS) and magnetron sputtering (MS) are summarized. Thin film growing models, the review of optical substrates polishing procedures and subsurface damages generation and elimination, the reasons of laser induced breakdown in optical materials are also provided.

## Chapter 2. Experimental techniques

Here, the experimental setups used in this work are described.

### Etching of FS substrates

The ordinary subsurface structure of polished FS substrate is presented in Fig. 1 a. The special etching gear (Fig. 1b) with bath for HF/HNO<sub>3</sub> acid etching of different durations was prepared and used to remove polished layer and clean out SSD containing slurry. By adding concentrated acid, such as HNO<sub>3</sub> to HF solutions, the etch rate is enhanced due to the catalytic role of H<sub>3</sub>O<sup>+</sup> ions in the dissolution process, on the other hand the cerium oxide is soluble in HNO<sub>3</sub>. Therefore, the removal of Bielby layer and SSD were expected.

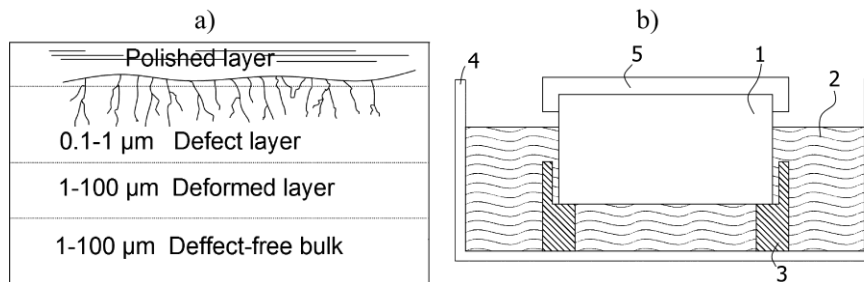


Fig. 1. Illustrations: surface structure in FS substrate (a), and etching procedure (b), where 1- substrate, 2- HF/HNO<sub>3</sub> acid mixture, 3- substrate holder, 4- etching bath, 5- hermetic cover.

The samples are placed on a special holder in an etching bath, where they are submerged up to 80% of substrate thickness in a hydrogen fluoride (HF) and nitric acid (HNO<sub>3</sub>) mixture. The hydrogen fluoride comprises 20% and the nitric acid 80% of the mixture. The sample of the unetched upper surface is hermetically secured (preventing deposition of dust or reaction with fumes from the etching solution) with a hermetic cover. The sample is allowed to soak for fixed durations. The temperature of the etching environment is maintained at 20°C and at 80% humidity. After the soaking phase the sample is rapidly removed from the acid solution and immediately rinsed with flowing distilled water.

### **Deposition of ZrO<sub>2</sub> films and Nb<sub>2</sub>O<sub>5</sub>/SiO<sub>2</sub> mixture thin films by reactive magnetron sputtering technique**

The deposition setups which were used for the deposition of ZrO<sub>2</sub> films and Nb<sub>2</sub>O<sub>5</sub>/SiO<sub>2</sub> mixture thin films are shown in Fig. 1. A Kurt J. Lesker sputtering system (PVD225) was equipped with a 4 inch diameter Torus<sup>TM</sup> sputter gun cathodes, which can be adjusted in angular position and z direction. A 6 mm thick, 101.6 mm diameter non-bonded Zr and Nb targets (purity - 99.95%) and 3 mm thick, 101.6 mm diameter Cu-bonded Si target were loaded in the sputter guns. The target-to-substrate distance ( $D_{TS}$ ) was  $200 \pm 2$  mm. The system was initially pumped down with a cryogenic pump (Cryo-Torr 8F series from Helix Technology Corporation; 1500 L/s air) to a base pressure below  $5 \times 10^{-7}$  Torr ( $6.7 \times 10^{-5}$  Pa). The ambient (Ar/O<sub>2</sub> or Ar/O<sub>2</sub>+N<sub>2</sub>) pressure during sputtering runs was always between 2.44 mTorr and 2.51 mTorr (0.325-0.335 Pa). All process gasses used for deposition were > 99.999 % pure and injected into the vacuum chamber through MKS Instruments MassFlo 1179A mass flow controllers (MFCs). The Ar flow rate was kept constant at 20 standart cm<sup>3</sup> (sccm). The Nb<sub>2</sub>O<sub>5</sub>/SiO<sub>2</sub> film composition was tuned by varying pulse-DC (p-DC) and RF power applied to the targets. The p-DC generator was operated at 100 kHz with 2  $\mu$ s off time (i.e. 80% duty cycle). The RF power supply for Si sputtering was operated at 13.56 MHz.

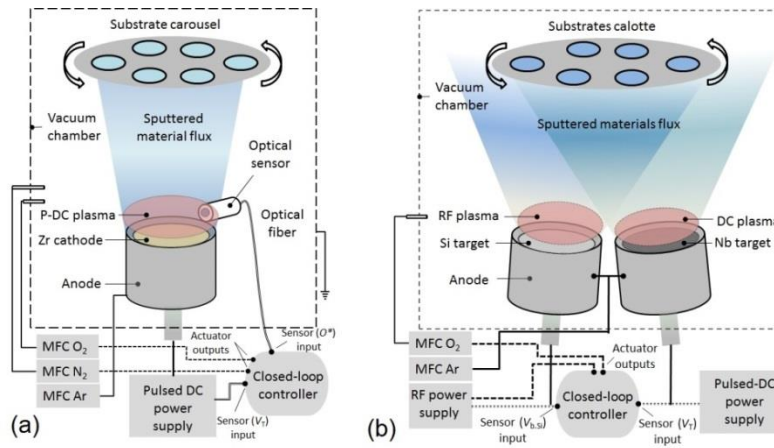


Fig. 2. Schematic diagram showing the process chamber used for: (a)  $ZrO_2$  films deposition, (b)  $Nb_2O_5/SiO_2$  mixture thin films.

Variables investigated in  $ZrO_2$  deposition study are i) the operating set-point in the reactive process window and ii) the nitrogen flow. The nitrogen gas content used in this work was calculated by taking the ratio of the  $N_2$  to  $O_2$  flow rate (both in sccm), and the values were varied from 0% to 37.5%.

A PID (proportional-integral-derivative)-based plasma monitoring controller was used to monitor and control the Zr-O sputtering process. Three feedback signals were employed: i) optical emission from the  $Zr^*$  spectral line at 351 nm, ii) optical emission from the spectral  $O^*$  line at 777 nm and target voltage,  $V_T$  (as an indicator of glow discharge impedance). All sensor and actuator signals were used (and logged) in a process window (i.e. a particular analog voltage range) and are presented normalised to 100%.

Fig. 3 a-b shows reactive gas flow ramp-up/down experiments that were needed to work out the process window for the deposition runs. In figure 3a an  $O_2$  flow ramp is executed and the corresponding changes in the sensor signals are recorded.  $Zr^*$   $O^*$  and  $V_T$  signals respond as expected. However, we should draw attention to the border values of the target voltage, which are  $\sim 76\%$  (upper) and  $7\%$  (lower). Importantly, these values could be obtained consistently by multiple consecutive  $O_2$  flow ramp experiments.

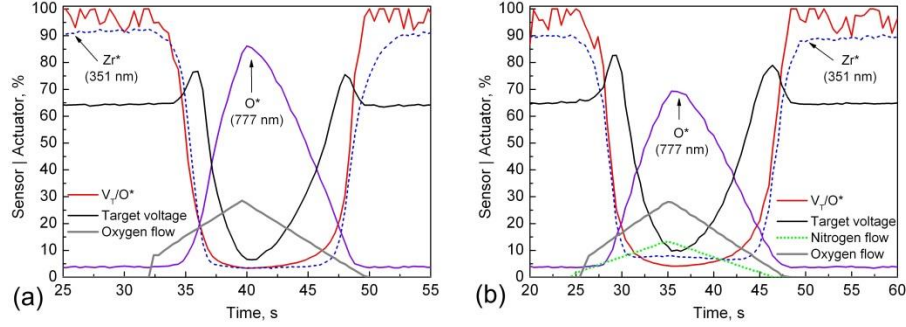


Fig. 3. Sensor and actuator signals during  $O_2$  – (a) and  $O_2 + N_2$  – (b) ramp experiments.  $N_2$  flow in this case follows  $O_2$  flow with an  $N_2/O_2$  ratio of 0.5. Sensors represents – Target Voltage ( $V_T$ ),  $O^*$  (777 nm),  $Zr^*$  (351 nm) and  $V_T/O^*$ .

Actuator –  $O_2$  or  $N_2$  MFC flow rate.

When  $N_2$  is introduced together with  $O_2$  flow (Fig. 3b), the behaviour changes slightly, but is essentially the same, which confirms complete oxidation of the racetrack as indicated by the sensors. This time, however,  $V_T$  upper and lower limits are  $\sim 82\%$  and  $10\%$ , respectively – i.e. a small shift in target voltage signal has occurred. Normally, the upper and lower values of the  $V_T$  signal correspond to process boundaries beyond which no process control yielding good quality stoichiometric films is possible.

The reactive gas flow during the Nb/Si sputtering processes was either not controlled (i.e. constant reactive gas flow) or controlled by an active feedback process control system. The oxygen flow rate for reactive MS processes with constant gas flow control (CFC) was determined on the basis of hysteresis, occurred at two direction of reactive gas flow (increasing and decreasing). A few repetitively  $NbO_x$  deposition processes were carried out at different oxygen flow rates until first relatively low absorption layer of  $Nb_2O_5$  was deposited (such an  $O_2$  flow rate in  $Nb_2O_5$  deposition was 14.0 sccm).

Reactive gas flow ramp-up/down experiments for Nb and Si processes are presented in Fig. 4. An  $O_2$  flow ramp is executed in pulsed-DC plasma and the corresponding changes in the sensor signals are shown in Fig. 4a. Classical responses of sensor signal ( $V_T$ ) are observed. Essentially the same oxygen ramp up/down experiment was carried out to characterize the RF  $SiO_2$  process. As shown in Fig. 4b, when oxygen is introduced, the bias voltage (sensor) exhibits a transition to the fully poisoned target state.



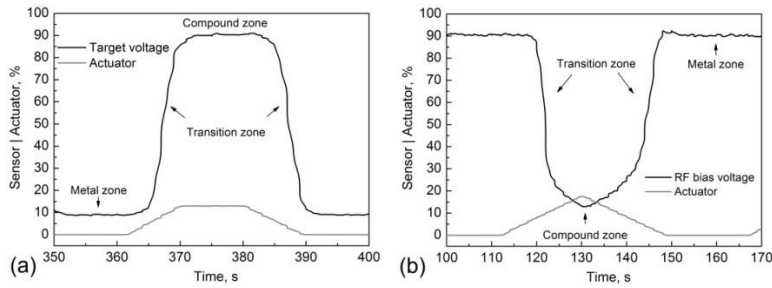


Fig. 4. Sensors ( $V_T$ ,  $V_{b,Si}$ ) and actuator ( $O_2$  MFC flow rate) signals during oxygen flow ramp up/down experiments in reactive pulsed-DC Nb (a) and RF Si (b) sputtering processes.

### Chapter 3. Investigation of Beilby (polished) layer

In this chapter, surface investigations of FS substrates, done by AFM, XPS is described. The presence of Beilby layer on polished FS surface was observed from AFM analysis in tapping phase image (Fig. 5a). Imaging in this mode reveals contaminant identification and mapping of components in composite materials. Hidden scratches filled with polishing slurry (or material different from the surrounding) are changing tapping phase signal which reveals invisible scratches in topography image (Fig. 5b). It confirms that during conventional abrasive polishing some digs and scratches are completely filled by residual polishing contaminants (polished layer). It was found that the AFM phase imaging is an easy and fast method to identify the Beilby layer. It can be involved in routine surface roughness measurements procedures.

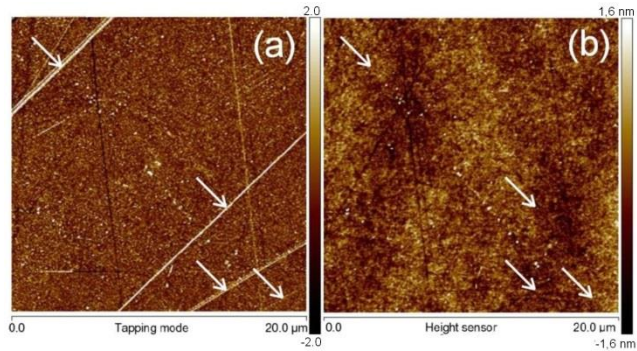


Fig. 5. AFM measurements: tapping phase image (a), topography of FS polished surface (b).

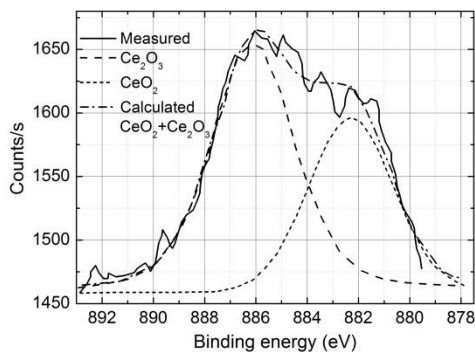


Fig. 6. Ce3d XPS spectra of conventional polished FS surface.

completely filled by residual polishing contaminants (polished layer). It was found that the AFM phase imaging is an easy and fast method to identify the Beilby layer. It can be involved in routine surface roughness measurements procedures.

To identify the presence of cerium abrasives in Beilby layer, XPS analysis was carried out. Typical XPS spectra of the core level Ce3d binding energies of conventionally polished FS surface are shown in Fig.

6. The measured XPS spectra are in good agreement with combined peaks of  $\text{CeO}_2$  and  $\text{Ce}_2\text{O}_3$  at their individual binding energies (883.8 eV and 886 eV, respectively). The intensity of XPS signal was very low. This is the outcome of very low concentration of cerium oxide contamination at the surface of polished FS. Depth profiling done by Kozlowski et. al. [1] showed that the majority of cerium contamination is located at the surface or at depth down to 30 nm and Ce concentration for the most polished FS was <30 ppm.

## Chapter 4. Influence of etching time on surface roughness and LIDT

In this section, influence of surface roughness and subsurface damages on the resistance of the FS substrates to laser radiation is investigated. Roughness of etched FS substrates (Fig. 7) is higher than of the ones that were not etched (RMS~0.41 nm). It is obvious that the etching of HF acid is irregular and the digs and scratches are deepening.

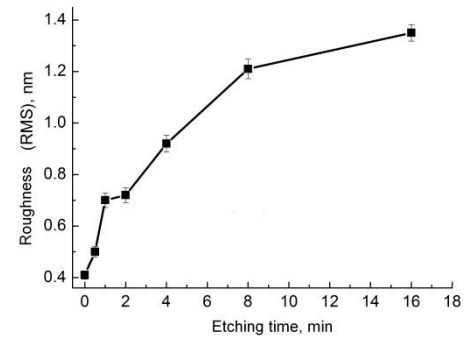


Fig. 7. Dependence of surface roughness on etching durations.

The LIDT of optics is known to be a subject sensitive to the type of abrasive polishing particles, their size and materials used. Particles absorbing laser light, such as abrasive grains, are often embedded within “Beilby” layer or within the subsurface damages and therefore are acting as damage precursors. The LIDT@355nm dependence on etching time of uncoated FS samples presented in Fig. 8a. Damage threshold measurements of etched (but not coated) fused silica substrates revealed, that the particular etching duration is required to achieve the highest resistance to UV laser radiation ( $\lambda=355$  nm, LIDT = 78 J/cm<sup>2</sup>). We determined that in our conditions this duration is ~ 1 min. All etched samples have significantly higher damage threshold (from 2.3 to 2.9 times) than the ones that were not etched. However, the LIDT values for durations of etching of 0.5 min and more than 1 minute, varies very smoothly (from 39% to 31% lower than in case of ~1 min etching duration) and appears near the limits of measuring errors. The effect of etching on commercially polished and  $\text{SiO}_2$  deposited samples can be seen from laser induced

damage morphologies. The characteristic damages of non-etched and acid-etched FS, coated SiO<sub>2</sub> layer, are presented here in Fig. 8 b,c. It has been revealed that for non-etched surface defects most likely associate with cerium oxide particles within Beilby layer (Fig. 8b), while damage morphology in 1 min etched FS sample had no visible point defects (Fig. 8c).

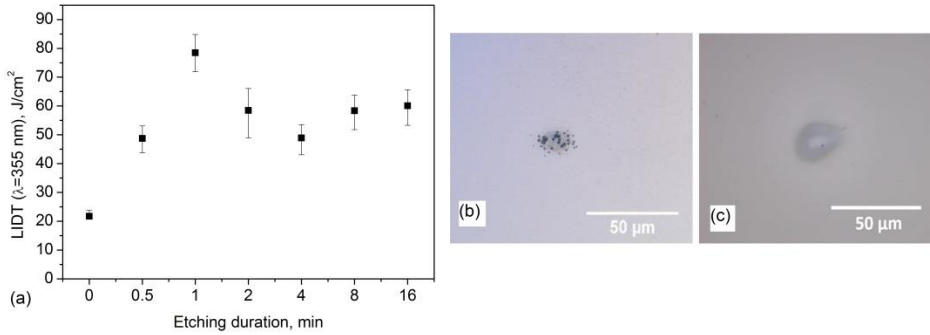


Fig. 8. The LIDT@355 dependence on etching time (a) and characteristic damages of FS coated SiO<sub>2</sub> layer: (a)-polished, (b)-1 min acid etched.

Despite small increase of surface roughness, optimal etching time was found to be ~1 min at given HF/HNO<sub>3</sub> acids mixture. The increment in LIDT up to a factor 4 was observed for conventionally polished fused silica substrates.

## Chapter 5. Coating designs with variable gradient refractive index

### *AR coatings on LBO crystals*

In this section, the coating materials ZrO<sub>2</sub> and SiO<sub>2</sub> were utilized for the synthesis of materials mixtures. The goal of the investigation was to explore the potential of ZrO<sub>2</sub>/SiO<sub>2</sub> mixtures especially for applications in the UV spectral range. The following designs of experimental AR coatings on LBO crystals were selected for examination:

- a) Regular discrete refractive index profile – LBO/L<sub>buf</sub>HL...HL/AIR, where L – SiO<sub>2</sub>, L<sub>buf</sub> – 31 nm buffer layer of SiO<sub>2</sub>, H – ZrO<sub>2</sub>-SiO<sub>2</sub>mix (30% or 20% of ZrO<sub>2</sub>) or pure Al<sub>2</sub>O<sub>3</sub>;
- b) Different “Rugate type” designs with variable gradient refractive index profile where the highest percentage of ZrO<sub>2</sub> in the mixture layers was also 30% and the lowest – 20%.

Primarily single antireflective UV coating for 355nm with enhanced transmission at 532 nm and 1064 nm wavelengths was investigated (AR<sub>355</sub>+HT<sub>532+1064</sub>). Since the pure ZrO<sub>2</sub> material has increased absorption losses close to resonance absorption edge (at 355nm

wavelength), we used  $\text{ZrO}_2\text{-SiO}_2$  mixtures that allows shifting that edge towards UV range and reduce absorption losses: the band-gap of the mixture materials are strongly varying with the content of  $\text{SiO}_2$ . Previous investigations showed, that increasing the  $\text{SiO}_2$  portion in the mixture to up to 50% leads to a blue shift of the absorption edge by approximately 40 nm [28]. On the other hand, content of  $\text{ZrO}_2$  in the mixture cannot be too low, because it is necessary to have sufficient contrast ratio of refractive indices of coating materials to achieve very low residual reflection ( $<0.1\%$ ) of the AR coating. Due to this, our AR coatings were designed by using minimal  $\text{ZrO}_2$  content of 20-30% in the mixture.  $\text{Al}_2\text{O}_3$  has the smallest UV absorption among all high refractive index oxide materials and is widely used in UV coatings. Since the  $\text{ZrO}_2\text{-SiO}_2$  mixture materials can reach similar to those of pure  $\text{Al}_2\text{O}_3$  band-gap and absorption properties we also wanted to compare their LIDT performance on LBO crystals. It should be also noted, that all AR coatings, despite used materials ( $\text{Al}_2\text{O}_3$  or  $\text{ZrO}_2\text{-SiO}_2$  mixtures) were designed using similar reflectance criteria.

Based on primary investigation with single wavelength antireflective coating, we designed an optimized AR coating for frequency-doubled and tripled wavelengths by using (20-30)%  $\text{ZrO}_2\text{-SiO}_2$  mixtures instead of pure oxides and having low  $<(0.1\text{-}0.3)\%$  residual reflection. The profiles of refractive indices and reflection spectra of designed coatings are shown in Fig. 9.

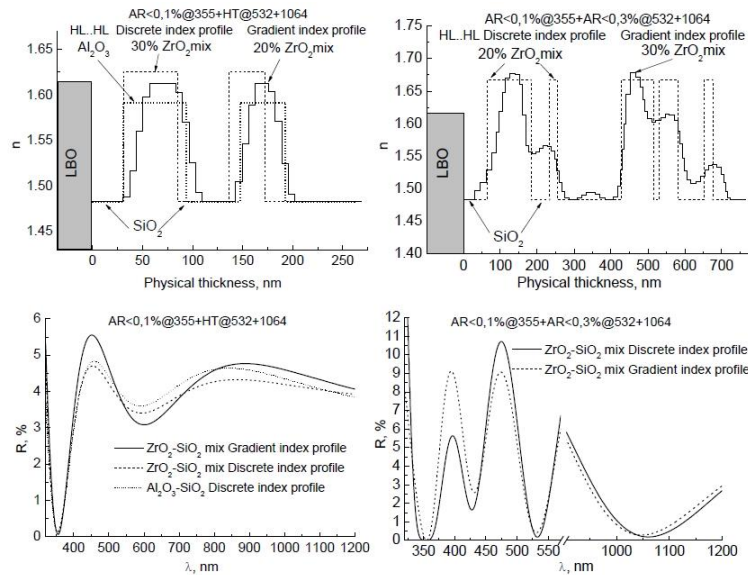


Fig. 9. Calculated refractive index profiles and spectras of  $\text{AR}_{355+\text{HT}_{532+1064}}$  (left) and  $\text{AR}_{355+532+1064}$  (right) coatings on LBO.

Automated S-on-1 (1000-on-1) measurements of LIDT's were performed according ISO 11254-2 norm [50]. LIDT of ZrO<sub>2</sub>-SiO<sub>2</sub> mixture based AR coatings were higher than based on Al<sub>2</sub>O<sub>3</sub>/SiO<sub>2</sub> layers (Table 1). This result can be explained by possible incomplete stoichiometry of Al<sub>2</sub>O<sub>3</sub> films in the coating and its microstructure inhomogeneity. Annealing of Al<sub>2</sub>O<sub>3</sub> based coatings at high temperature could improve optical and resistance properties, but the LBO crystals are too sensitive to high temperatures, so annealing procedure was not possible.

Table 1 Optical parameters of various AR coating designs and summary results of LIDT.

Coating	R <sub>355</sub> , %	R <sub>532</sub> , %	R <sub>1064</sub> , %	LIDT*, J/cm <sup>2</sup>	
				10 Hz	6 kHz
(ZrO <sub>2</sub> -SO <sub>2</sub> mix.) Discr. AR <sub>355</sub> +HT <sub>532+1064</sub>	0.11	3.8	4.0	11.3	8.8
(Al <sub>2</sub> O <sub>3</sub> /SiO <sub>2</sub> ) Discr. AR <sub>355</sub> +HT <sub>532+1064</sub>	0.14	4.1	4.2	10.9	4.8
(ZrO <sub>2</sub> -SO <sub>2</sub> mix.) Grad. AR <sub>355</sub> +HT <sub>532+1064</sub>	0.07	4.0	4.5	5.2	5.6
(ZrO <sub>2</sub> -SO <sub>2</sub> mix.) Discr. AR <sub>355+532+1064</sub>	0.06	0.1	0.2	-	7.5
(ZrO <sub>2</sub> -SO <sub>2</sub> mix.) Grad. AR <sub>355+532+1064</sub>	0.07	0.4	0,3	8.4	10.2

\*LIDT (1000-on-1) parameters:  $\lambda=355$  nm,  $\tau=8,7$  ns, beam diameter – 38  $\mu$ m.

### *Notch filter*

The gradient index design was realized with the ion beam sputtering (IBS) system (Cutting Edge Coatings GmbH). Transmittance spectrum and refractive index profile of *Notch* filter, composed of 600 layers, each ~ 8.3 nm in thickness, is presented in Fig. 10. The refractive index contrast ( $\Delta n$ ) of 0.24 was selected, which determines a narrow area of low transmission, i.e. spectrum width of 28 nm at  $\lambda_0=426$  nm in the transmission height of 30%. The *rugate* zone of 39 modulated cycles was a partially apodised Gaussian function. Partial apodisation was performed at two thickness zones: between 0.5 $\mu$ m to 2 $\mu$ m and 3 $\mu$ m to 5 $\mu$ m of the coating's physical thickness. The middle layer between 2 $\mu$ m and 3 $\mu$ m was not apodised resulting in thinner coating and smaller refractive index contrast, which allowed us to achieve as little permeability to 426nm wavelength as possible. Likewise, a 5<sup>th</sup> degree polynom of the assimilation areas was used for the *Notch* filter.

The comparison of transmission spectra between theoretically modelled and manufactured *Notch* filter showed that in the latter the zone of low transmission was deeper

and wider by  $\sim 8\text{nm}$  (at the transmission height of 30%). It had a lower transmission for the 426nm wavelength than predicted ( $T= 0.82\%$  vs  $T=2.72\%$ ). After the reverse engineering process the refractive index profile for the *Notch* filter was calculated. It appeared that the actual refractive index contrast increased by 25% (from 0.24 to  $0.30\pm 0.01$ ) According to theory, the depth and width of the low transmission zone in  $\lambda/4$ -thick discrete layers as well as in *rugate* coating structures is determined by the refraction index contrast. This is also the case in the present observation.

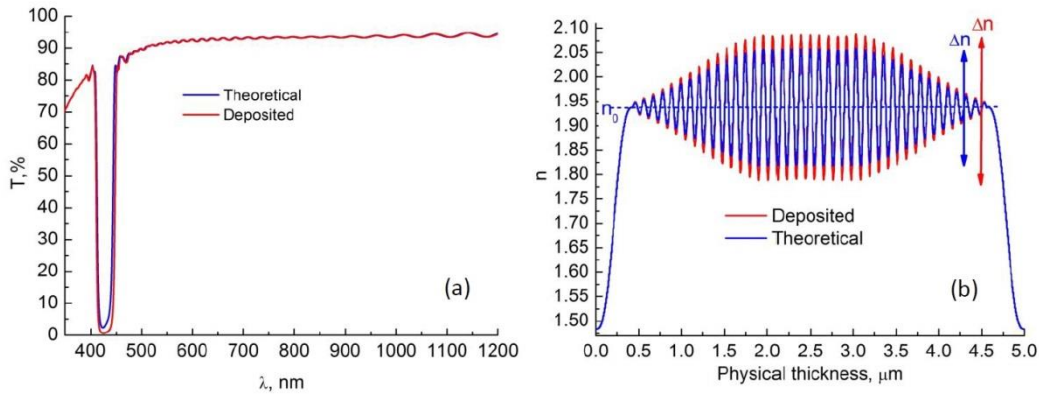


Fig. 10. Transmittance spectrum (a) and refractive index profile (b) of *Notch* filter.

This discrepancy can be explained by the indeterminacy of the technological process, which is influenced by the calibration of the zone target. Indeterminacy is introduced in repetitive sputtering processes when the initial conditions in the sputtering chamber are not always identical. Temperature, vacuum and humidity – all have a major influence on the primary properties of optical coatings. It is well known, that when the chamber is opened at normal conditions (room temperature, atmosphere pressure) the walls of the chamber, which are already coated with various particles and coatings, tend to absorb humidity and a certain film forms. When the chamber is closed and vacuumed again, and a new process of reactive sputtering is started, the refractive index of the manufactured coatings varies. To avoid these effects, some deposition technologies utilize pre-heating of the chamber walls at high temperature ( $300^{\circ}\text{C}$ ). This step removes humidity and improves the vacuum formation. However, IBS technology that we utilize does not have a pre-heating option, therefore all processes were started at room temperature. This could have contributed to the minor spectral inconsistencies of the filters. The changes of refractive index can sometimes be

0.5% as the coating layers grow. Consequently, even a small refractive index deviation from the theoretical (calibration curve) influences the final spectral errors of the filter. Despite this, we have successfully demonstrated *rugate* coating with unique spectral properties: narrow filters with high transmission efficiency in the wide spectral range.

## Chapter 6. Investigations of ZrO<sub>2</sub> thin films deposited by reactive magnetrons sputtering

### ZrO<sub>2</sub> reactive sputtering

Experiments carried out in this study (using target voltage control) have led to a discovery that operation beyond the top maximum  $V_T$  value (as indicated by reactive process characterisation tests described in chapter 2) is not only possible, but can yield coatings with good optical properties (low  $k$  and high  $n$ ) at a higher deposition rate. In particular, figure 11a shows data collected during an experiment designed specifically to demonstrate this phenomenon. Here reactive Zr sputtering in O<sub>2</sub>/Ar atmosphere is controlled using a  $V_T/O^*$  ratio as a feedback signal. The target is fully oxidised initially (period from 0 to 40 s) after which the set-point is ramped up gradually to move the process up the transition region. The full extent of the phenomenon demonstrated in figure 11a can be seen in figure 11b, where sensor signals are plotted against time during one of the deposition runs. The process shown in figure 11b is controlled using the  $V_T/O^*$  ratio, for which the set-point was 42%. The

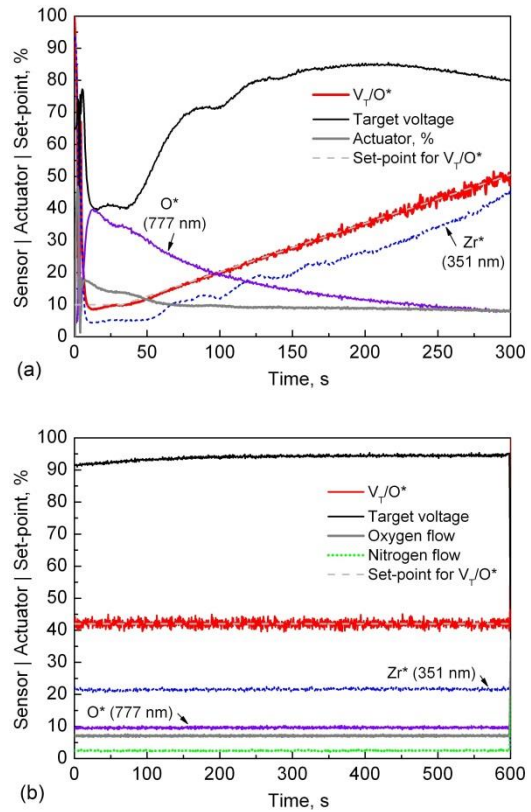


Fig. 11. Process control experiment in which the set-point for the  $V_T/O^*$  ratio is ramped from 10% (transition region near ‘fully poisoned’ mode) to over 50% (transition region near ‘metal’ zone) (a) and an example of process data from a deposition run where the  $V_T/O^*$  ratio is used for closed-loop gas flow control (b).

target voltage is above 90% at all times and exceeds 93% during the majority of the run. Such operation was found to yield consistently the best process (in terms of deposition rate) and coatings (in terms optical properties) and has therefore been used for deposition of all films.

Results of this study as well as those published previously by Depla et al. [51] indicate that the Zr target voltage exhibits a complex behaviour when oxygen is introduced into a discharge plasma. This behaviour is essentially governed by changes in the Ion Induced Secondary Electron Emission (ISEE) [51]. ISEE depends strongly on the nature of compounds formed in the racetrack - as well as on coverage, impacting ion energy, etc. If the hypothesis of Depla et al. [51] is correct, then our data for Zr target voltage behaviour shown in figure 3 means that the Zr target poisoning process undergoes several transitions, such as ‘metal-to-suboxide’ and ‘suboxide-to-oxide’. These transitions in the racetrack chemical composition can be seen in the  $V_T$  signal, but there is no sign of them in optical emission signals -  $O^*$  and  $Zr^*$  (figure 3). We found that the best optical quality coatings are produced when the  $V_T$  is at the very maximum, i.e. racetrack is wholly or partially covered with (possibly) a suboxide. Remarkably, the target voltage can be pushed even higher (as shown in figures 3 and 11), yielding further improved deposition rate and film properties.

The best performance (i.e. optimal process conditions) is obtained using  $V_T$  over  $O^*$  (at 777 nm) ratio. If a single feedback signal (e.g.  $O^*$  or  $Zr^*$ ) is used, as in conventional plasma emission monitoring (P.E.M.), maximum performance of the process, in terms of deposition rate and optical film properties, is not obtained.

### *ZrO<sub>2</sub> Deposition rate*

Closed-loop gas flow control enabled high deposition rates of zirconium oxide films at 800W applied target power and  $D_{TS} = 20$  cm, which varied from 3.9 Å/s to 6.4 Å/s; this corresponds to between 39 % and 64 % of pure metal deposition rate, respectively. The highest deposition rates are obtained when using the  $V_T/O^*$  ratio as a feedback signal. Without closed-loop gas flow control at the same  $D_{TS}$ , the deposition rate varied from 0.13 Å/s to 0.5 Å/s at 250 W and 500 W applied power, respectively. Experimental results collected in this investigation confirm earlier findings, i.e. that active feedback process



control is necessary to make the most of the transition between different target states phenomenon. When compared to prevalent EB [52] and IBS [24] technologies it becomes clear that the deposition process developed in this study provides superior coatings at very high deposition rates.

*XPS analysis and microstructure of ZrO<sub>2</sub>*

XPS analysis revealed that nitrogen incorporation in the zirconia film is low (2.1 and 4.5 at. %), even if the N<sub>2</sub> flow is relatively high (25 % and 37.5 % in respect of oxygen). Similar a low amount of nitrogen incorporated in zirconia film has been reported in earlier work [47]. This can be explained by the higher reactivity of oxygen which favours the formation of metal–oxygen bonds over metal–nitrogen bonds.

Figure 12 shows X-ray diffractograms of ZrO<sub>2</sub> films deposited at different oxygen and nitrogen ratios. From XRD patterns it was determined that the films crystallize in a double - phase of monoclinic/tetragonal when N<sub>2</sub>=0% and monoclinic/rhombohedral when N<sub>2</sub>=12.5% - 25% (in respect to oxygen). In the former case the predominant polycrystalline monoclinic phase has a (-111) crystallographic plane (corresponding diffraction peak at 2Θ=28.1°) oriented parallel to the surface. The heights of the monoclinic phase peaks, decreased and these of the rhombohedral increased with an increase in nitrogen concentration. The monoclinic phase peaks vanished when N<sub>2</sub>

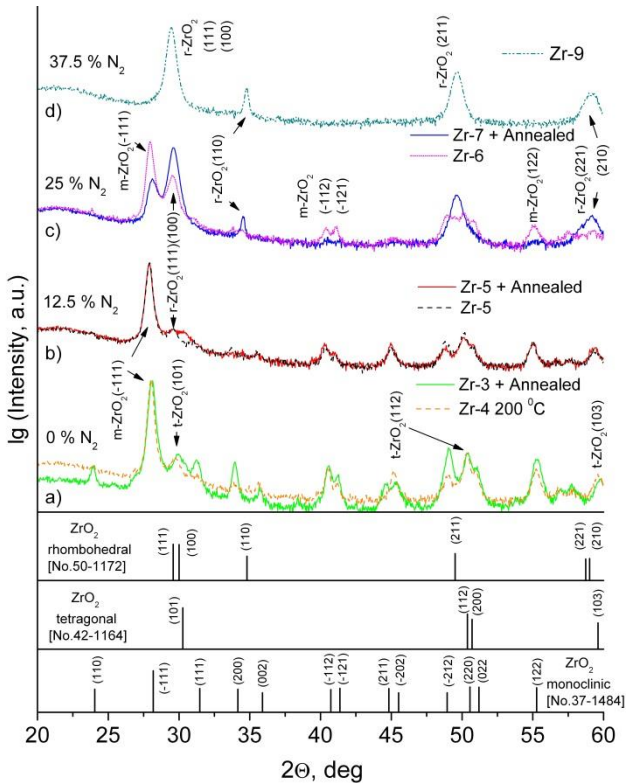


Fig. 12. X-ray diffraction patterns of ZrO<sub>x</sub>N<sub>y</sub> films prepared at different O<sub>2</sub>:N<sub>2</sub> ratio.

reached 37.5 % of the gas flow in the magnetron chamber. It should be noted that the rhombohedral crystal structure is unusual for ZrO<sub>2</sub>. On the other hand, Zr<sub>7</sub>O<sub>8</sub>N<sub>4</sub> has mainly the rhombohedral crystal structure. The XRD patterns of studied layers are more alike that

of the rhombohedral  $ZrO_2$  but not like that of  $Zr_7O_8N_4$ . However, the lattice parameters of the rhombohedral  $ZrO_2$  in the current layers were slightly different from those presented in PDF No. 50-1172:  $a = 3.613 \text{ \AA}$ ,  $c = 9.09 \text{ \AA}$  and  $a = 3.643 \text{ \AA}$ ,  $c = 9.05 \text{ \AA}$ , respectively. The variations of lattice parameters could be caused by the insertion of nitrogen into the crystal lattice of  $ZrO_2$ . The presence of nitrogen in the layers was confirmed by the XPS analysis.

The monoclinic phase of  $ZrO_2$  is in agreement with earlier papers [42, 47]. Hasegawa et.al. [53] have demonstrated that the phase transformation from stable cubic to rhombohedral can occur if growing zirconia film is subjected to  $N_2$  ion implantation. However, rhombohedral zirconia is not a form known as well as some rhombohedral oxynitride phases, such as  $Zr_7O_{11}N_2$  and  $Zr_7O_8N_4$ , which contain large quantity of nitrogen (the atomic ratio:  $N/O = 2/11$  and  $1/2$ ).

Nitrogen concentration in  $ZrO_2$  film caused by implantation corresponds only to a ratio  $N/O$  of  $\sim 1/200$ . Therefore the authors [53] conclude that the rhombohedral  $ZrO_2$  phase produced by the  $N_2$  implantation is not an oxynitride phases. This supports our results well as  $N_2$  concentration in our samples is very low (up to max 4.5 at. %); the XRD patterns of studied layers also resemble more the rhombohedral  $ZrO_2$  structure rather than that of  $Zr_7O_8N_4$ .

#### *Optical properties of $ZrO_2$ thin films*

Figure 13 presents the dispersion of the refractive index ( $n$ ) and extinction coefficient ( $k$ ) derived from analysis of the transmittance spectra for selected  $ZrO_x$  and  $ZrO_xN_y$  films deposited at different oxygen (a, b) and nitrogen (c, d) partial pressures. It was found that  $k$  and therefore  $n$  of the films slightly increased upon increasing nitrogen incorporation. Thin films deposited without feedback control are strongly influenced by thermal treatment, i.e. annealing effect or deposition at high (200 °C) temperature. This is due to incomplete oxidation during slow (0.13 Å/s or 0.15 Å/s) deposition. The lowest extinction coefficient was established in sample deposited at 200 °C. This result is not satisfactory, because there is a requirement to deposit optical coatings on laser crystals or other glasses at temperatures up to 80 °C.

Closed-loop control allowed the deposition of stoichiometric  $ZrO_2$  thin films exhibiting a relatively low extinction coefficient (0.001 against 0.0003; respectively sample 3 and sample 2) and without additional thermal treatment, i.e. substrate heating or annealing (Fig. 13b). The refractive index ( $> 2.15$ ) of such  $ZrO_2$  layer (eg. sample 3) is also attractive for high index contrast broadband mirrors or complicated coating designs like narrow band filters or *rugate* filters, where the refractive index changes when film is growing.

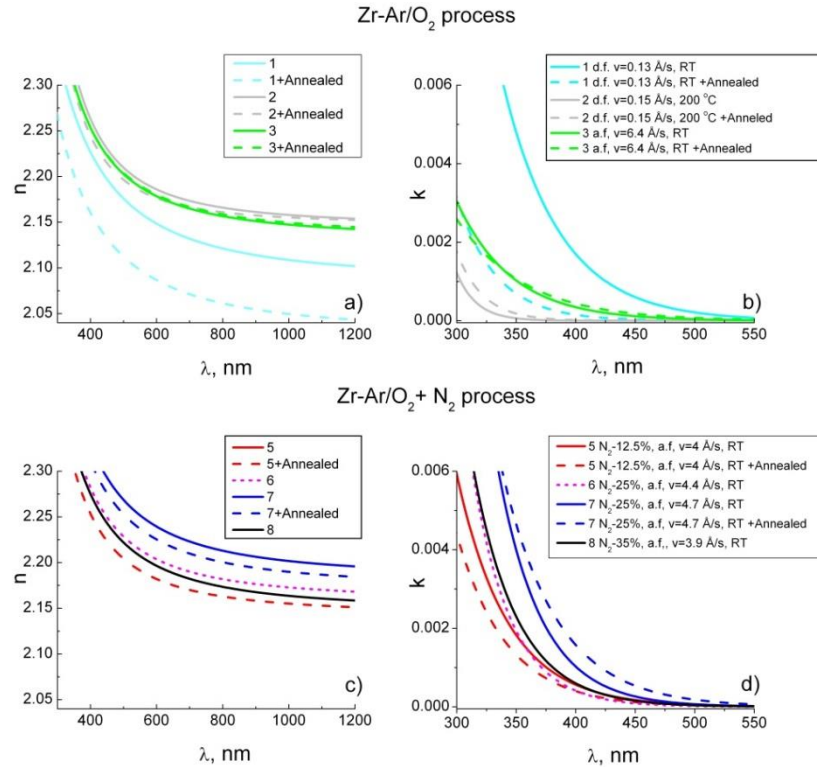


Fig. 13. Refractive index and extinction coefficient dispersions of  $ZrO_2$  films deposited by reactive sputtering with and without active feedback process control.

## Chapter 7. Investigation of $Nb_2O_5/SiO_2$ mixture thin films deposited by reactive magnetron sputtering technique

### *Formation of $Nb_2O_5/SiO_2$ mixture thin films*

A linear  $Nb_2O_5$  fraction in the  $Nb_2O_5/SiO_2$  mixture dependence on RF (Si) and pulsed-DC (Nb) power levels is revealed (shown in Fig. 14). Data points in were obtained by reactive sputtering with closed-loop process control. This dependence allows easy process parameter selection and accurate regulation of any fraction of the two oxide materials

chosen, thus any refractive index in the range between pure niobia and silica can be obtained, which is particularly valuable and applicable for the production of optical coatings with a gradient refractive index profile.

### Deposition rate

Deposition rates of pure  $\text{Nb}_2\text{O}_5$ ,  $\text{SiO}_2$  and their mixtures deposited by the two reactive sputtering processes used in this study are shown in Fig. 15. As expected, active feedback-based control (CLC) allowed 61% and 137% higher deposition rates of  $\text{Nb}_2\text{O}_5$  and  $\text{SiO}_2$  layers respectively, as compared to reactive magnetron sputtering with constant oxygen flow.

### Optical film properties

The dispersion of the refractive index ( $n$ ) and extinction coefficient ( $k$ ) derived from analysis of the transmittance spectra for selected  $\text{Nb}_2\text{O}_5/\text{SiO}_2$  mixture thin films are presented in Fig. 16. It was found that the optical constants of pure oxide materials or respective mixtures are almost identical for both process control methods.

The dispersion of extinction coefficient (Fig. 16 b and d) of the films shows that the absorption edge is shifted towards lower wavelengths as the amount of  $\text{SiO}_2$  in the mixture increases. The optical band gap values vary in a range between  $E_g = 3.46$  eV for pure niobium oxide and  $E_g = 4.03$  eV for 22%  $\text{Nb}_2\text{O}_5$  fraction. Determined band gaps

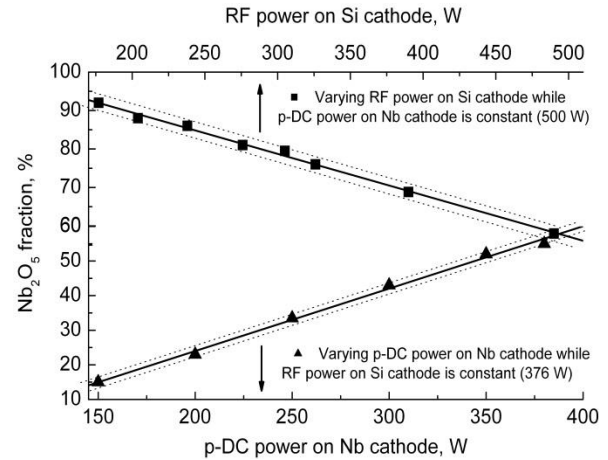


Fig. 14. mixtures was determined by varying RF and pulsed-DC power levels. Data points were obtained by reactive sputtering with closed-loop process control.

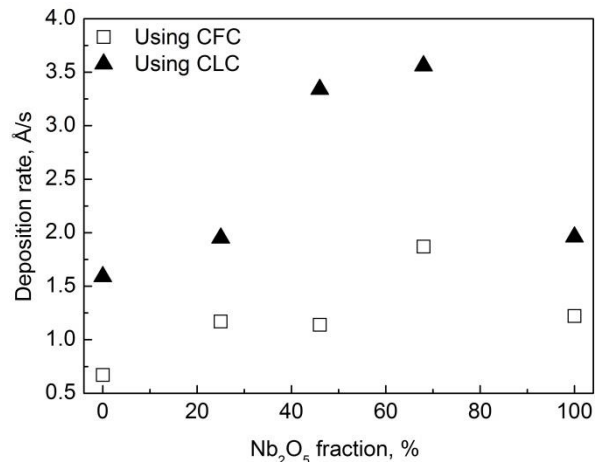


Fig. 15. The deposition rates of pure oxide materials ( $\text{Nb}_2\text{O}_5$ ,  $\text{SiO}_2$ ) and their mixtures deposited using two different reactive sputtering process control methods.

correlate in limit of errors between two different process control methods. Pure niobium pentoxide has identical band gap values when deposited by both control methods.

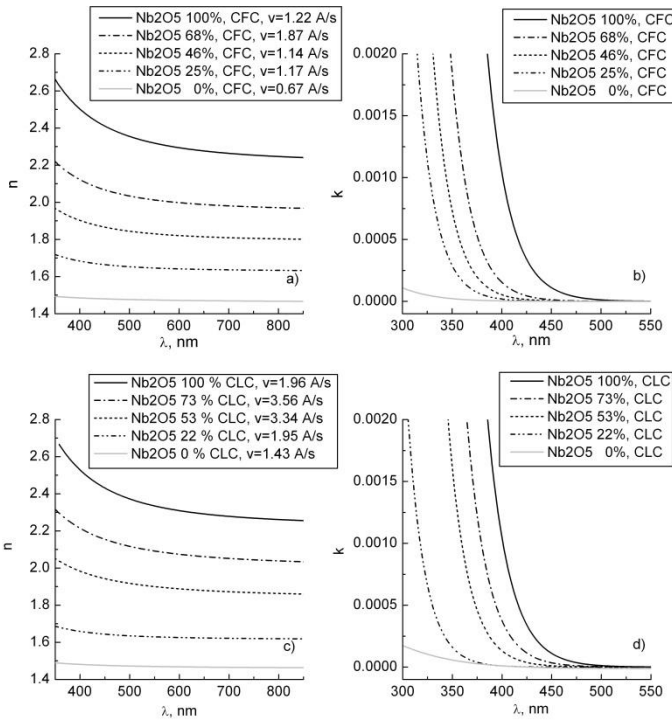


Fig. 16. Refractive index and extinction coefficient dependence on the wavelength of  $\text{Nb}_2\text{O}_5/\text{SiO}_2$  mixtures deposited by reactive sputtering with constant  $\text{O}_2$  flow control (CFC) (a,b) or with closed-loop (CLC) process control (c,d).

Refractive index gradients (inhomogeneity) are a crucial matter when preparing optical thin films, especially with mixed oxides. When the refractive index is decreasing with increasing thickness of the layer, the refractive index gradient is said to be ‘negative’. This investigation showed that reactive deposition in fully poisoned mode leads to negative inhomogeneity, which varies from -1.2% in

The optical properties like refractive index and band-gap are easily tuned between the pure materials values using the deposition technique described in this work. Therefore production of rugate filters is possible with nearly continuous refractive index profile by simply changing p-DC/RF power at determined  $V_T$  set-points during the deposition process.

Importantly, a significantly higher inhomogeneity of refractive index was found in mixtures deposited with no feedback control (Fig. 17), as a result of process instabilities when operating in ‘fully-poisoned’ mode.

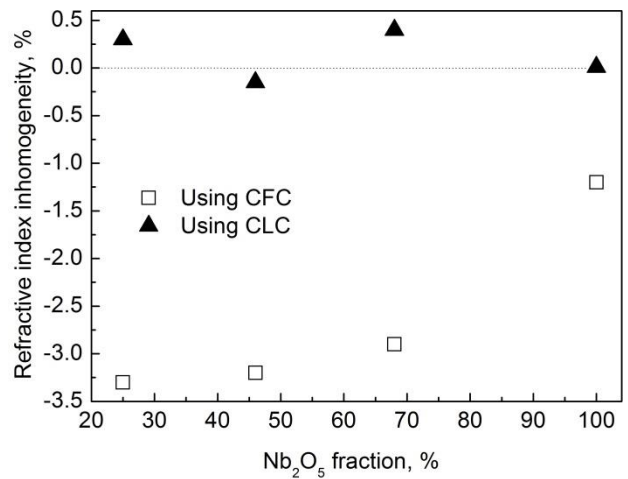


Fig. 17. Refractive index inhomogeneity of  $\text{Nb}_2\text{O}_5/\text{SiO}_2$  mixtures deposited with constant  $\text{O}_2$  flow and with closed-loop control.

pure  $\text{Nb}_2\text{O}_5$  to -3.3% in film with 25% fraction of niobium pentoxide. From figure 17 can be seen that negative inhomogeneity increases with increase  $\text{SiO}_2$  content in mixture. We attribute this effect to a variation of the  $\text{SiO}_2$  porosity in the depth of the mixture layer. Mixtures of high  $\text{SiO}_2$  content were deposited at relatively high flow of oxygen, i.e. in 'compound' zone of Nb target to ensure niobium oxidation (Table 1). Therefore, Si target was strongly oxidised and sputtering in strongly poisoned target state affected formation of porous mixture thin film. By contrast, a maximum of only 0.4% positive inhomogeneity was found for deposition in the 'transition' zone by employing closed-loop process control. We attribute this effect to the high stability of the deposition conditions during sputtering, which appears to result in a constant film composition along the mixture thin film.

## Conclusions

1. Chemical analysis of the commercially polished substrates surface showed that the Beilby's layer and sub-surface defects consisted of the remnants of the polishing materials (particles of  $\text{CeO}_x$ ). The remnants were distributed unevenly, as the change of particle's concentration throughout the surface of the FS substrate was observed.
2. The methodology of chemical etching in the  $\text{HF}/\text{HNO}_3$  solution was developed. It allows to etch the Beilby's layer and to remove the remnants of the polishing material located in the micro-cracks. However, increasing duration of etching increases the surface roughness of the optical substrate.
3. An optimal time of acid etching in the 20%  $\text{HF}$  and 80%  $\text{HNO}_3$  solution was determined to be 1 min. It increases the laser induced damage threshold of etched fused silica substrates by a factor of 4.
4. Antireflective coatings with gradient refractive index were deposited on the non-linear LBO crystals by ion beam sputtering. The usage of  $\text{ZrO}_2/\text{SiO}_2$  mixtures allowed to reduce the total quantity of  $\text{ZrO}_2$  in the coating and to increase its resistance to UV laser radiation.  $\text{SiO}_2$  sub-layer further increased resistance to laser radiation by 10%.

5. Coating, based on  $\text{ZrO}_2\text{-SiO}_2$  mixtures, with gradient refractive index was deposited by ion beam sputtering technique. It had unique spectral properties: narrow area of high reflection and high transmission in the wide wavelength range.
6. Research on reactive magnetron sputtering showed anomalies in the Zr target voltage response at the changing reactive gas flow. It was shown that closed-loop reactive gas control with combined sensor ( $V_T/O^*$ ) is the only way to control the process of reactive Zr sputtering at the abnormal target voltage response.
7. Usage of combined  $V_T/O$  sensor in the process of reactive magnetron sputtering, allowed to increase the  $\text{ZrO}_2$  deposition rate approximately 43 times, compared to the processes where constant reactive gas flow control was used. Layers of  $\text{ZrO}_2$  which were formed in the temperature between  $20^\circ\text{C}$  and  $40^\circ\text{C}$  had low losses ( $k=0.001$  at  $\lambda=350$  nm) and high refractive index ( $n=2.15$  ( $\lambda=1000$  nm)). Such optical characteristics are attractive for high contrast of refractive index broadband mirrors.
8. Absorption losses in  $\text{ZrO}_2$  thin films, deposited by using constant  $\text{O}_2$  flow control, were significantly decreased after thermal annealing at  $300^\circ\text{C}$  temperature. This shows that if constant flow control of reactive gas is applied during sputtering, the oxidation of zirconium is incomplete. Annealing procedure did not affect the layers deposited using an active feedback  $\text{O}_2$  control and shows complete zirconium oxidation during deposition process.
9. As shown by structural analysis of X-ray diffraction, Zr sputtering in the  $\text{O}_2$  atmosphere makes zirconium oxide to form polycrystalline monoclinic-tetragonal mixture phases. Sputtering in the  $\text{O}_2+\text{N}_2$  atmosphere, on the other hand, causes the formation of monoclinic-rhombohedral mixture phases or pure rhombohedral polycrystalline phase.
10. Nitrogen concentration in the  $\text{ZrO}_x\text{N}_y$  thin films was very low (up to 4.5 at.%) despite relatively large flow of nitrogen during reactive magnetron sputtering (12%-37.5% in relation to oxygen) was used.

11. Deposition rate of Nb<sub>2</sub>O<sub>5</sub> and SiO<sub>2</sub> layers, which were deposited by reactive magnetron sputtering with closed-loop reactive gas flow control, was higher by 61% and 137%, respectively, as compared to constant reactive gas flow control.
12. Nb<sub>2</sub>O<sub>5</sub>/SiO<sub>2</sub> mixed oxide films, deposited by reactive magnetron sputtering, were amorphous in structure. The roughness of their surface depended only on the roughness of the substrates.
13. Significantly reduced refractive index inhomogeneity of mixtures was found when using active-feedback controlled reactive sputtering process, i.e. only up to max 0.4% positive inhomogeneity was found for deposition in the ‘transition’ zone. Compared, reactive deposition in ‘fully poisoned’ regime leads to negative inhomogeneity in films which varies from -1.2% to -3.3%.

## References

1. M. R. Kozlowski, J. Carr, I. D. Hutcheon, R. A. Torres, L. M. Sheehan, D. W. Camp, and M. Yan, "Depth profiling of polishing-induced contamination on fused silica surfaces," *Proc. SPIE* **3244**, 365-375 (1998).
2. P. E. Miller, T. I. Suratwala, L. L. Wong, M. D. Feit, J. A. Menapace, P. J. Davis, and R. A. Steele, "The distribution of subsurface damage in fused silica," *Proc. SPIE* **5991**, 599101-599125 (2005).
3. Y. Lee, "Evaluating subsurface damage in optical glasses," *J. Eur. Opt. Soc.* **6**(2011).
4. J. A. Menapace, P. J. Davis, W. A. Steele, L. L. Wong, T. I. Suratwala, and P. E. Miller, "MRF applications: measurement of process-dependent subsurface damage in optical materials using the MRF wedge technique," *Proc. SPIE* **5991**, 599103 (2005).
5. C. L. Battersby, L. M. Sheehan, and M. R. Kozlowski, "Effects of wet etch processing on laser-induced damage of fused silica surfaces," *Proc. SPIE* **3578**, 446-455 (1999).
6. T. I. Suratwala, P. E. Miller, J. D. Bude, W. A. Steele, N. Shen, M. V. Monticelli, M. D. Feit, T. A. Laurence, M. A. Norton, C. W. Carr, and L. L. Wong, "HF-Based Etching Processes for Improving Laser Damage Resistance of Fused Silica Optical Surfaces," *J. Am. Ceram. Soc.* **94**, 416-428 (2011).
7. S. Li, Z. Wang, and Y. Wu, "Relationship between subsurface damage and surface roughness of optical materials in grinding and lapping processes," *J. Mater. Process. Technol.* **205**, 34-41 (2008).
8. J. Shen, S. Liu, K. Yi, H. He, J. Shao, and Z. Fan, "Subsurface damage in optical substrates," *Optik* **116**, 288-294 (2005).
9. J. Lambropoulos, "From abrasive size to subsurface damage in grinding," in *OSA Technical Digest (Optical Society of America, 2000)*, OMA6.
10. J. H. Campbell, "Damage Resistant Optical Glasses for High Power Lasers: A Continuing Glass Science and Technology Challenge," UCRL-JC-149843 (2002).
11. L. Hongjie, H. Jin, W. Fengrui, Z. Xinda, Y. Xin, Z. Xiaoyan, S. Laixi, J. Xiaodong, S. Zhan, and Z. Wanguo, "Subsurface defects of fused silica optics and laser induced damage at 351 nm," *Opt. Express* **21**, 12204-12217 (2013).
12. S. Liukaitytė, G. Batavičiūtė, E. Pupka, M. Ščiuka, I. Kraujalienė, D. Tumosa, A. Skrebutėnas, K. Juškevičius, T. Tolenis, S. Kičas, R. Drazdys, R. Buzelis, and A. Melninkaitis, "Effect of conventional fused silica preparation and deposition techniques on surface roughness, scattering, and laser damage resistance," *Proc. SPIE* **8530**, 853027-853027 (2012).



13. N. Bloembergen, "Role of Cracks, Pores, and Absorbing Inclusions on Laser Induced Damage Threshold at Surfaces of Transparent Dielectrics," *Appl. Opt.* **12**, 661-664 (1973).
14. M. D. Feit and A. M. Rubenchik, "Influence of subsurface cracks on laser-induced surface damage," *Proc. SPIE* **5273**, 264-272 (2004).
15. S. Jha and V. K. Jain, "Nanofinishing Techniques," in *Micromanufacturing and Nanotechnology* (Springer Berlin Heidelberg, 2006), pp. 171-195.
16. J. A. Menapace, B. Penetrante, D. Golini, A. F. Slomba, P. E. Miller, T. G. Parham, M. Nichols, and J. Peterson, "Combined advanced finishing and UV-laser conditioning for producing UV-damage-resistant fused-silica optics," *Proc. SPIE* **4679**, 56-68 (2002).
17. Y. Li, H. Huang, R. Xie, H. Li, Y. Deng, X. Chen, J. Wang, Q. Xu, W. Yang, and Y. Guo, "A method for evaluating subsurface damage in optical glass," *Opt. Express* **18**, 17180-17186 (2010).
18. P. E. Miller, T. I. Suratwala, J. D. Bude, T. A. Laurence, N. Shen, W. A. Steele, M. D. Feit, J. A. Menapace, and L. L. Wong, "Laser damage precursors in fused silica," in (SPIE 7504, 2009), 75040X-75014.
19. D. Poitras, J. A. Dobrowolski, T. Cassidy, and S. Moisa, "Ion-Beam Etching for the Precise Manufacture of Optical Coatings: Erratum," *Appl. Optics* **42**, 5749-5749 (2003).
20. J. Neauport, L. Lamaignere, H. Bercegol, F. Pilon, and J. C. Birolleau, "Polishing-induced contamination of fused silica optics and laser induced damage density at 351 nm," *Opt. Express* **13**, 10163-10171 (2005).
21. R. M. Brusasco, B. M. Penetrante, J. E. Peterson, S. M. Maricle, and J. A. Menapace, "UV-laser conditioning for reduction of 351-nm damage initiation in fused silica," *Proc. SPIE* **4679**, 48-55 (2002).
22. E. Lorenzo, C. J. Oton, N. E. Capuj, M. Ghulinyan, D. Navarro-Urrios, Z. Gaburro, and L. Pavesi, "Porous silicon-based rugate filters," *Appl. Opt.* **44**, 5415-5421 (2005).
23. K. Starke, T. Grob, and D. Ristau, "Rapid prototyping of optical thin film filters," *Proc. SPIE* **4094**, 83-92 (2000).
24. A. Melnikaitis, T. Tolenis, L. Mazule, J. Mirauskas, V. Sirutkaitis, B. Mangote, X. Fu, M. Zerrad, L. Gallais, M. Commandré, S. Kicas, and R. Drazdys, "Characterization of zirconia and niobia silica mixture coatings produced by ion-beam sputtering," *Appl. Opt.* **50**, C188-C196 (2011).
25. L. O. Jensen, M. Mende, H. Blaschke, D. Ristau, D. Nguyen, L. Emmert, and W. Rudolph, "Investigations on SiO<sub>2</sub>/HfO<sub>2</sub> mixtures for nanosecond and femtosecond pulses," *Proc. SPIE* **7842**, 784207-784207 (2010).
26. W. H. Southwell, "Gradient-index antireflection coatings," *Opt. Lett.* **8**, 584-586 (1983).
27. W. H. Southwell and R. L. Hall, "Rugate filter sidelobe suppression using quintic and rugated quintic matching layers," *Appl. Opt.* **28**, 2949-2951 (1989).
28. K. Starke, L. O. Jensen, M. Jupé, D. Ristau, G. Abromavicius, K. Juškevičius, R. Buzelis, and R. Drazdys, "Investigation in oxide mixture coatings with adapted gradient index profiles," *Proc. SPIE* **7504**, 75040B (2009).
29. S. Chao, W.-H. Wang, and C.-C. Lee, "Low-Loss Dielectric Mirror with Ion-Beam-Sputtered TiO<sub>2</sub>-SiO<sub>2</sub> Mixed Films," *Appl. Opt.* **40**, 2177-2182 (2001).
30. B. J. Pond, J. I. DeBar, C. K. Carniglia, and T. Raj, "Stress reduction in ion beam sputtered mixed oxide films," *Appl. Opt.* **28**, 2800-2805 (1989).
31. S. Bruns and M. Vergöhl, "Optical and thin film properties of mixed oxides deposited by pulsed reactive magnetron sputtering," *Proc. SPIE* **8168**, 81680N-81680N (2011).
32. D. Rademacher, G. Bräuer, B. Fritz, and M. Vergöhl, "Optical properties of silicon titanium oxide mixtures prepared by metallic mode reactive sputtering," *Appl. Opt.* **51**, 8047-8051 (2012).
33. X. Fu, A. Melnikaitis, L. Gallais, S. Kicas, R. Drazdys, V. Sirutkaitis, and M. Commandré, "Investigation of the distribution of laser damage precursors at 1064 nm, 12 ns on Niobia-Silica and Zirconia-Silica mixtures," *Opt. Express* **20**, 26089-26098 (2012).
34. C. Chen, Y. Wu, A. Jiang, B. Wu, G. You, R. Li, and S. Lin, "New nonlinear-optical crystal: LiB<sub>3</sub>O<sub>5</sub>," *J. Opt. Soc. Am. B* **6**, 616-621 (1989).

35. D. A. Keszler, "Borates for optical frequency conversion," *Curr. Opin. Solid State Mater. Sci.* **1**, 204-211 (1996).
36. E. A. Levchuk, V. V. Novopashin, and A. V. Shestakov, "High-quality interference coatings for LBO and BBO crystals produced by the ion-beam technique," *Proc. SPIE* **3738**, 118-125 (1999).
37. Z. Deng, H. Gao, L. Xiao, H. He, Z. Fan, and J. Shao, "Design and preparation of frequency doubling antireflection coating with different thicknesses of interlayer for LiB<sub>3</sub>O<sub>5</sub> crystal," *Chin. Opt. Lett.* **5**, 60-62 (2007).
38. J. Musil, J. Vjcek, and P. Baroch, "Magnetron Discharges for Thin Films Plasma Processing," in *Materials Surface Processing by Directed Energy Techniques*, 1 ed., Y. Pauleau, ed. (Elsevier Verlag, 2006), pp. 67-110.
39. M. Audronis, "Reactive Sputtering: Basic Concepts of Reactive Sputtering" (2013), retrieved 2013, <http://www.reactive-sputtering.info/node/99>.
40. E. Hollands and D. S. Campbell, "The mechanism of reactive sputtering," *J. Mater. Sci.* **3**, 544-552 (1968).
41. M. Audronis, V. Bellido-Gonzalez, and B. Daniel, "Control of reactive high power impulse magnetron sputtering processes," *Surf. Coat. Technol.* **204**, 2159-2164 (2010).
42. S. Venkataraj, O. Kappertz, R. Jayavel, and M. Wuttig, "Growth and characterization of zirconium oxynitride films prepared by reactive direct current magnetron sputtering," *J. Appl. Phys.* **92**, 2461-2466 (2002).
43. M. Scherer, J. Schmitt, R. Latz, and M. Schanz, "Reactive alternating current magnetron sputtering of dielectric layers," *J. Vac. Sci. Technol., A* **10**, 1772-1776 (1992).
44. S. Schiller, K. Goedicke, J. Reschke, V. Kirchhoff, S. Schneider, and F. Milde, "Pulsed magnetron sputter technology," *Surf. Coat. Technol.* **61**, 331-337 (1993).
45. M. Audronis, K. Juškevičius, R. Drazdys, and A. Matthews, "Unlocking the potential of voltage control for high rate zirconium and hafnium oxide deposition by reactive magnetron sputtering," *Proc. 12th Int. Symp. ISSP2013 (Kyoto, Japan, 10-12 July)* (2013).
46. K. Juškevičius, M. Audronis, A. Subačius, R. Drazdys, R. Juškėnas, A. Matthews, and A. Leyland, "High-rate reactive magnetron sputtering of zirconia films for laser optics applications," *Appl. Phys. A*, 1-12 (2014).
47. D. Severin, K. Sarakinos, O. Kappertz, A. Pflug, and M. Wuttig, "Tailoring of structure formation and phase composition in reactively sputtered zirconium oxide films using nitrogen as an additional reactive gas," *J. Appl. Phys.* **103**, 083306-083305 (2008).
48. J. Park, J. K. Heo, and Y. C. Kang, "The Properties of RF Sputtered Zirconium Oxide Thin Films at Different Plasma Gas Ratio," *B. Kor.Chem. Soc.* **31**, 397-400 (2010).
49. S. Venkataraj, O. Kappertz, H. Weis, R. Drese, R. Jayavel, and M. Wuttig, "Structural and optical properties of thin zirconium oxide films prepared by reactive direct current magnetron sputtering," *J. Appl. Phys.* **92**, 3599-3607 (2002).
50. ISO-11254-2, "Lasers and laser-related equipment," in *Determination of laser-induced damage threshold of optical surfaces, Part 2: S-on-I test*, (2001).
51. D. Depla, S. Heirwegh, S. Mahieu, J. Haemers, and R. De Gryse, "Understanding the discharge voltage behavior during reactive sputtering of oxides," *J. Appl. Phys.* **101**, 013301-013309 (2007).
52. A. Melninkaitis, D. Mikšys, T. Balčiūnas, V. Sirutkaitis, A. Skrebutėnas, R. Buzelis, R. Drazdys, and G. Abromavičius, "Effect of substrate temperature and ion assistance on nanosecond laser-induced damage threshold in high reflection dielectric coatings," *Proc. SPIE* **5991**, 59911B (2005).
53. H. Hasegawa, T. Hioki, and O. Kamigaito, "Cubic-to-rhombohedral phase transformation in zirconia by ion implantation," *J Mater Sci Lett* **4**, 1092-1094 (1985).

## CURRICULUM VITAE

Name, Surname: **Kęstutis Juškevičius**

Date of birth and place: **1983 07 18**, Panevėžys, Lithuania

Education: **2002** Panevėžio “Žemynos” secondary school  
**2006** Physics Bachelor Degree of Vilnius University  
**2008** Physics Master Degree of Vilnius University  
**2009-2013** PhD studies at the Center for Physical Sciences and  
Technology, Institute of Physics, Lithuania

## Santrauka

Disertacijos tikslas buvo nustatyti fizikines priežastis, ribojančias dielektrinių optinių dangų spektrinius parametrus bei jų atsparumą lazerio spinduliuotei ir pateikti įvairių jų gamybos etapų – optinių pagrindukų paruošimo dengimo procesui, optinių dangų struktūros bei dengimo technologijų optimizavimo rekomendacijas optinių komponentų gamintojams.

Šiame darbe buvo atlikta komerciškai poliruotų kvarco pagrindukų visapusiška paviršiaus analize, kuri parodė, kad paviršiuje esama poliravimo medžiagų liekanų įstrigusių įvairiuose režiuose bei mikrotrūkiuose ir “paslėptų” po taip vadinamu Bilbio sluoksniu. Siekiant nuėsdinti šį sluoksnį ir pašalinti poliravimo medžiagų liekanas, buvo sukurta cheminio ėsdinimo HF/HNO<sub>3</sub> tirpale metodika. Nustatyta, kad chemiškai ėsdintų kvarco pagrindukų pažaidos lazerio spinduliuotei slenkstis padidėjo apie 4 kartus.

Šiame darbe didelis dėmesys buvo skiriamas naujų optinių dangų modelių paieškai ir dangų formavimui, panaudojant ZrO<sub>2</sub>/SiO<sub>2</sub> medžiagų mišinius. Panaudojant metalų oksidų mišinių plonuosius sluoksnius, buvo suformuotos didelio atsparumo skaidrinančios dangos ant netiesinių LBO kristalų bei didelio atspindžio periodiškai kintančio lūžio rodiklio optinės dangos ant kvarco pagrindukų.

Šiame darbe buvo pasirinktas magnetroninio dulkinimo technologijos, kuri yra santykinai nauja optinių dangų industrijoje, optimizavimas. Pirmą kartą pademonstruota reaktyvaus magnetroninio dulkinimo proceso valdymas, panaudojant kombinuotą reaktyviųjų dujų jutiklį. Jo pagalba buvo suformuoti mažų sugerties nuostolių bei didelio lūžio rodiklio ir tankio ZrO<sub>2</sub> sluoksniai, bei Nb<sub>2</sub>O<sub>5</sub>/SiO<sub>2</sub> mišiniai, esant didelei sluoksnių augimo spartai. Pateiktos rekomendacijos, siekiant padidinti reaktyvinių magnetroninio dulkinimo procesų stabilumą.